



|                                     |  |
|-------------------------------------|--|
| <b>Title</b>                        | Spray deposited NiOx films on ITO substrates as photoactive electrodes for p-type dye-sensitized solar cells   |
| <b>Authors(s)</b>                   | Awais, Muhammad, Dowling, Denis P., Rahman, Mahfujur, Vos, Johannes G., Decker, Franco, Dini, Danilo   |
| <b>Publication date</b>             | 2013-02  |
| <b>Publication information</b>      | Awais, Muhammad, Denis P. Dowling, Mahfujur Rahman, Johannes G. Vos, Franco Decker, and Danilo Dini. "Spray Deposited NiOx Films on ITO Substrates as Photoactive Electrodes for P-Type Dye-Sensitized Solar Cells." Springer, February 2013.<br><a href="https://doi.org/10.1007/s10800-012-0506-1">https://doi.org/10.1007/s10800-012-0506-1</a> . |
| <b>Publisher</b>                    | Springer   |
| <b>Item record/more information</b> | <a href="http://hdl.handle.net/10197/4197">http://hdl.handle.net/10197/4197</a>  |
| <b>Publisher's statement</b>        | The final publication is available at <a href="http://www.springerlink.com">www.springerlink.com</a>   |
| <b>Publisher's version (DOI)</b>    | 10.1007/s10800-012-0506-1  |

Downloaded 2026-05-01 23:34:07

The UCD community has made this article openly available. Please share how this access benefits you. Your story matters! (@ucd\_oa)



© Some rights reserved. For more information

## Spray deposited NiO<sub>x</sub> films on ITO substrates as photoactive electrodes for *p*-type dye-sensitized solar cells

Muhammad Awais,<sup>a,b,c</sup> Denis P. Dowling,<sup>a,b</sup> Mahfujur Rahman,<sup>a,d</sup> Han Vos,<sup>a,e</sup> Franco Decker,<sup>f</sup> Danilo Dini<sup>a,f\*</sup>

*a: Solar Energy Conversion Strategic Research Cluster*

*b: School of Mechanical and Materials Engineering, University College Dublin, Ireland*

*c: Interdisciplinary Research Centre in Biomedical Materials (IRCBM), COMSATS Institute of Information Technology (CIIT), Defence Road, Off Raiwind Road, Lahore, Pakistan*

*d: School of Chemical and Bioprocess Engineering, University College Dublin, Ireland*

*e: School of Chemical Sciences, Dublin City University, Ireland*

*f: Dept. of Chemistry, University of Rome "La Sapienza", P.le Aldo Moro 5, 00185 Rome, Italy*

*\*corresponding author (email: [danilo.dini@uniroma1.it](mailto:danilo.dini@uniroma1.it); fax: +39-06-490324)*

### Abstract

Spray deposition followed by sintering of nickel oxide (NiO<sub>x</sub>) nanoparticles (average diameter: 40 nm) has been chosen as method of deposition of mesoporous NiO<sub>x</sub> coatings onto indium tin oxide (ITO) glass substrates. This procedure allows the scalable preparation of NiO<sub>x</sub> samples with large surface area (~ 10<sup>3</sup> times the geometrical area) useful for applications like electrocatalysis or electrochemical solar energy conversion that require high electroactivity in confined systems. The potential of these NiO<sub>x</sub> films as semiconducting cathodes for dye-sensitized solar cells (DSCs) purposes has been evaluated for 0.3-3 μm thick films of NiO<sub>x</sub> sensitized with erythrosine B (ERY). The electrochemical processes involving the NiO<sub>x</sub> coatings in the pristine and sensitized states result surface-confined as proved by the linear dependence of the current densities with the scan rate of the cyclic voltammetry. Cathodic polarization of NiO<sub>x</sub> on ITO can also lead to the irreversible reduction of the underlying ITO substrate due to the mesoporous nature of sintered NiO<sub>x</sub> film that allows the shunting of ITO to the electrolyte. ITO-based reduction processes alter irreversibly, the properties of charge transfer through the ITO/NiO<sub>x</sub> interface and limit the range of potential to NiO<sub>x</sub> coatings sintered for DSCs purposes.

**Keywords:** nickel oxide • *p*-type semiconductor electrode • semiconductor electrochemistry • dye-sensitized solar cell • indium tin oxide • sintering

## 1. Introduction

Nickel oxide ( $\text{NiO}_x$  with  $1 < x < 1.5$ ) is a *p*-type semiconductor with wide band-gap ( $E_g > 3.50$  eV) displaying room temperature conductivity values in the order of  $10^{-4}$  -  $10^{-2}$  S  $\text{cm}^{-1}$ .<sup>[1]</sup> The intrinsic *p*-type conductivity of  $\text{NiO}_x$  is mainly related to its non-stoichiometric nature where  $\text{Ni}^{3+}$  centers constitute the oxide defects through which holes are transferred.<sup>[2]</sup> Moreover, the oxide is characterized by high chemical stability and optical transparency when in the configuration of thin film with thickness,  $l < 2$   $\mu\text{m}$ ).<sup>[3,4]</sup> Because of this interesting combination of electrical and optical properties,  $\text{NiO}_x$  has been considered as active material for various applications like energy storage, <sup>[5,6]</sup> in electrochromic smart windows, <sup>[7-11]</sup> optoelectronic devices,<sup>[12]</sup> and, more importantly, in dye-sensitized solar cells (DSCs) as photoactive dye-sensitized mesoporous cathode.<sup>[13-19]</sup> The utilization of  $\text{NiO}_x$  in such diverse applications has been accompanied by the development of various preparation methods and deposition techniques aimed at producing  $\text{NiO}_x$  based materials with variable chemical composition, electrical resistivity, compactness and morphology for performance optimization. Most common examples include sputtering,<sup>[20]</sup> electrochemical deposition,<sup>[21]</sup> spray pyrolysis <sup>[22]</sup> or sol-gel method.<sup>[13,23,24]</sup> In the present work we have considered the fabrication of  $\text{NiO}_x$  thin films ( $0.2 < l < 3$   $\mu\text{m}$ ) for DSC purposes through the thermal sintering of spray deposited  $\text{NiO}_x$  nanoparticles (average diameter 40 nm) onto indium-tin oxide (ITO) glass substrates. The determination of the morphological, electrochemical and photo-electrochemical properties of  $\text{NiO}_x$  films in the bare state and in the sensitized version with dye erythrosine B (ERY),<sup>[13,24]</sup> has been accomplished together with the analysis of the electrochemical processes occurring in uncoated ITO substrates.<sup>[25,26]</sup> This approach allows the critical evaluation of the factors regulating the performance of the DSCs based on photoactive cathodes of sintered  $\text{NiO}_x$  when deposited onto ITO through a scalable method.

## 2. Experimental part

### 2.1 Deposition of $\text{NiO}_x$ coatings

$\text{NiO}_x$  nanoparticles, with an average particle size of 40 nm (from Sigma-Aldrich) were suspended in 2-propanol (concentration: 20 mg/mL). A loosely adherent particulate layer of  $\text{NiO}_x$  was then

deposited from this suspension by spray deposition, using a technique similar to that described previously by Halme *et al.* [27,28]. The nanoparticle layer was deposited onto unheated ITO-coated glass panels (5 cm x 5 cm) obtained from Balzers. The NiO<sub>x</sub> nanoparticles on the conducting glass substrate were sintered for 30 minutes using a Carbolite Furnace (RHF 1200), in air at 450 °C. [27] This thermal treatment affords the connection of the NiO<sub>x</sub> nanoparticles and warrants the electrical contact between nanoparticles and at the NiO<sub>x</sub>/ITO interface. By controlling the duration of spraying, the thickness of the NiO<sub>x</sub> nanoparticulate coatings on the ITO glass substrates was controlled as required in the range 0.3-3 μm.

### 2.2 Morphology characterization equipment

The cross sectional investigations of the NiO<sub>x</sub> coating were carried out using a FEI Quanta 3D FEG DaulBeam<sup>TM</sup> (FEI Ltd, Hillsboro, USA) focused ion beam/scanning electron microscope (FIB/SEM) system. Prior to SEM analyses, the deposited NiO<sub>x</sub> films were coated with platinum via sputtering using an Emitech K575X sputter coating unit. This was done in order to prevent surface charging by the electron beam.

### 2.3 Sensitization of NiO<sub>x</sub> coatings

NiO<sub>x</sub> coatings were sensitized with ERY from Sigma-Aldrich ( $\lambda_{MAX}$ : 535 nm), by dipping the oxide film in a 0.3 mM solution of the dye in 99.8 % ethanol (from Fisher) for 24 hrs at room temperature. After removing the electrode from tincture solution the sensitized electrode was washed with pure ethanol in order to remove the non chemisorbed dye molecules.

### 2.4 Electrochemical characterization of uncoated ITO

Prior to electrochemical cycling the uncoated ITO substrate was cleaned in an ultrasonic bath (solvent: isopropyl alcohol) for 30 mins and then dried in oven at 60 °C. After this cleaning treatment the ITO substrate was placed in the Ar filled glove box. The uncoated ITO substrate was manipulated in the glove-box for cell assembly.

### 2.5 Electrochemical characterization of NiO<sub>x</sub> coatings

The electrochemical cell was had had a three-electrode configuration [29] with glass/ITO/NiO<sub>x</sub> or dye-sensitized NiO<sub>x</sub> as working electrode, Li rod (from Sigma-Aldrich) as counter electrode, and Li / LiClO<sub>4</sub> [0.7 M in anhydrous propylene carbonate (PC) from Fisher] as reference electrode. All potential values in this work are referred to the Li<sup>+</sup>/Li redox couple. [30] Electrolyte was 0.7 M

LiClO<sub>4</sub> in anhydrous PC. Supporting electrolyte LiClO<sub>4</sub> was purchased from Aldrich and was not pre-treated before use. Chemicals were stored in an Ar filled glove-box (Innovative Technology, Newburyport, Massachusetts, USA) with O<sub>2</sub> and H<sub>2</sub>O content below 10 ppm and 5 ppm, respectively. The electrochemical cells were assembled under Ar atmosphere inside the glove-box and a supernatant Ar atmosphere was maintained in the cell during the electrochemical experiments with bare and sensitized NiO<sub>x</sub> samples. Cyclic voltammeteries were carried out using an electrochemical analyzer (model 604C) from CH Instruments (Austin, Texas, USA).

### *2.6 DSCs preparation*

The sensitized films (see Section 2.3) were sealed face-to-face in a sandwich configuration with a platinised ITO counter electrode using 30µm thick pre-cut Surlyn thermoplastic frame (6 × 6 mm interior) similar to what is reported in ref.31. The sandwiched device was filled with 0.1M I<sub>2</sub> and 1.0M LiI in acetonitrile electrolyte through a pre-drilled hole in the counter electrode using an insertion procedure at reduced pressure.[32] The hole was sealed with Surlyn and a glass cover-slide.

## **3. Results and Discussion**

### *3.1 Electrochemical behavior of sintered NiO<sub>x</sub> coating on ITO*

The SEM pictures images of a 2.7 micron thick sample (Figures 1 and 2), demonstrate that the NiO<sub>x</sub> coatings on ITO deposited using the spray technique, followed by furnace sintering, exhibit a relatively rough surface morphology and mesoporous features.

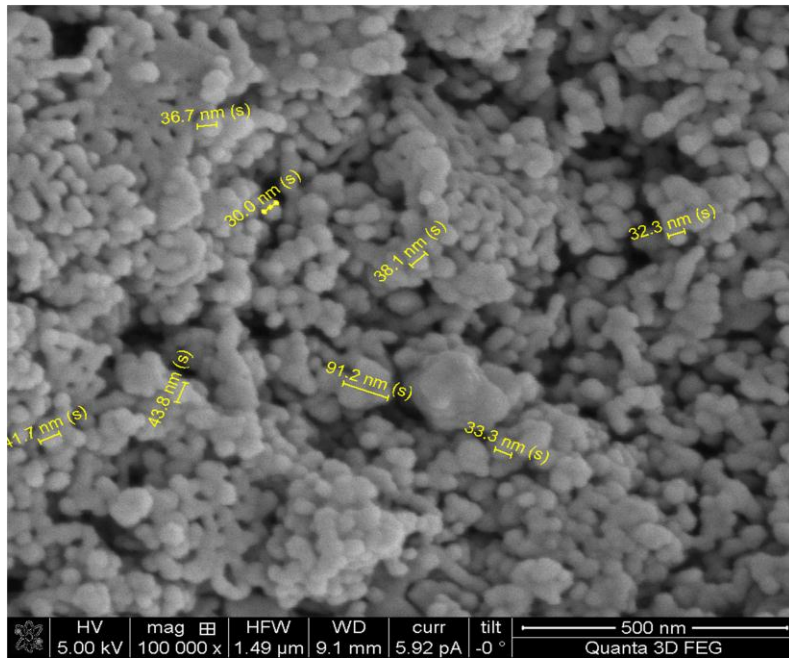


**Figure 1.** SEM image showing the surface morphology of a NiO<sub>x</sub> layer ( $l = 2-3 \mu\text{m}$ ) deposited onto ITO via sintering of nanoparticles with diameter values distributed between 30 and 90 nm (evidenced in yellow).

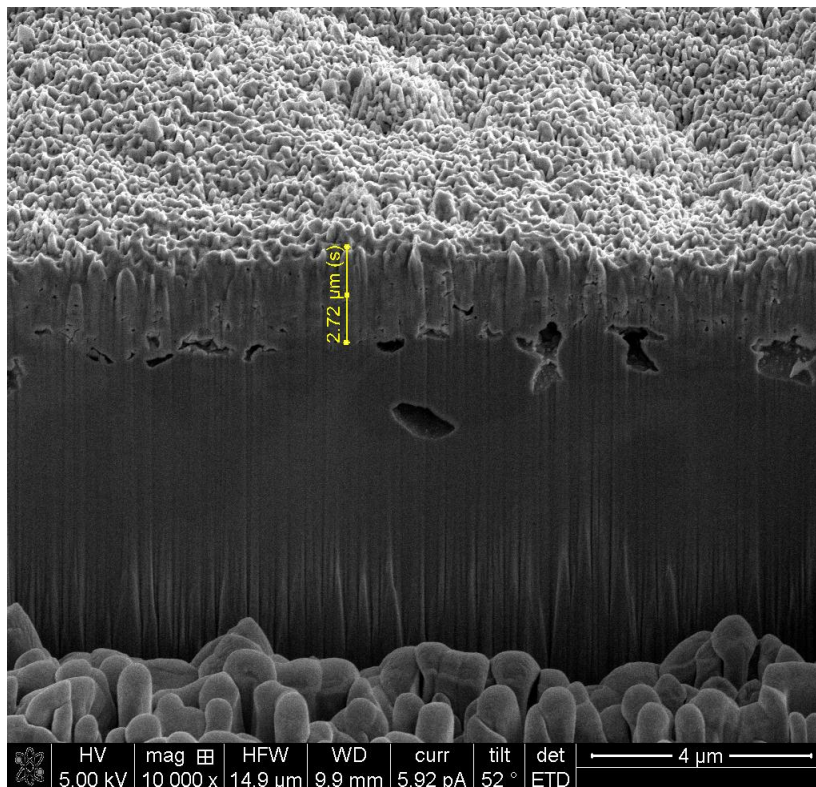


**Figure 2.** Dual beam FIB-SEM image showing the cross-section of a NiO<sub>x</sub> layer ( $l = 2-3 \mu\text{m}$ ) deposited onto ITO via conventional sintering of nanoparticles with average diameter of 40 nm (Figure 1). Yellow arrow indicates the thickness of the NiO film.

The NiO<sub>x</sub> film deposited onto ITO via conventional sintering of 40 nm diameter oxide nanoparticles,[27] presents a voltammogram typical of NiO<sub>x</sub> thin coatings with two broad oxidation waves in the interval 2.75-3.75 V vs Li<sup>+</sup>/Li,[33] and lithium ions intercalation in the potential range 1-2.5 V vs Li<sup>+</sup>/Li [34,35] (Figure 3, first cycle).

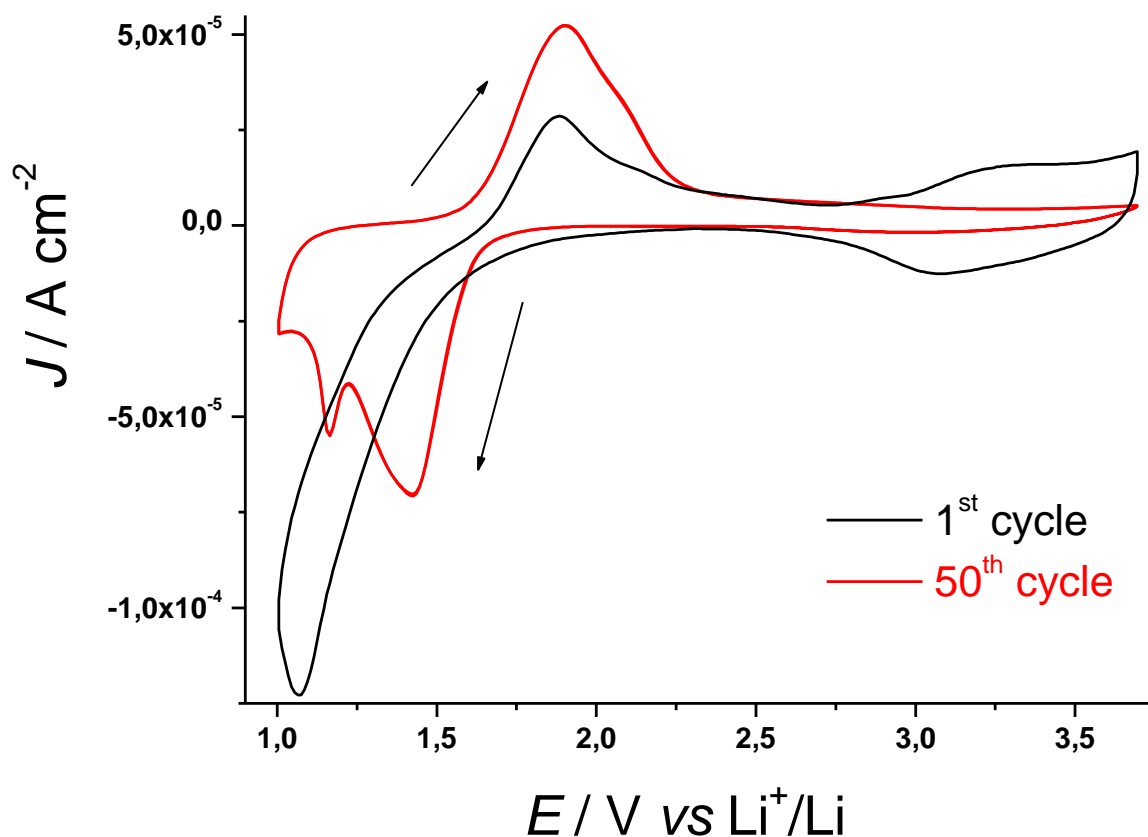


**Figure 3.** Effect of electrochemical cycling on the voltammogram of NiO<sub>x</sub>-coated ITO (scan rate: 15 mV s<sup>-1</sup>). Electrolyte: 0.7 M LiClO<sub>4</sub> in anhydrous PC; counter electrode: Li; reference redox couple: Li<sup>+</sup>/Li. Thickness of NiO<sub>x</sub> coating: 0.3 μm.

Continuous cycling in the extended potential range 1-4 V vs Li<sup>+</sup>/Li leads to the loss of any electrochemical feature characteristic of NiO<sub>x</sub> oxidation ( $E > 2.5$  V vs Li<sup>+</sup>/Li) and to the thorough modification of the shape of the reduction peak (Figure 3). This indicates that *n*-type ITO modifies its electron transfer properties upon electrochemical cycling [36] also in non-aqueous electrolyte due to the direct contact of ITO with the electrolyte. Such a shunt effect is due to the porous nature of sintered NiO<sub>x</sub> coating (Figures 1 and 2), which allows the formation of the ITO/electrolyte interface. The electrochemical behavior of uncoated ITO in 0.7 M LiClO<sub>4</sub> -PC (sheet resistance: 15 Ω/□, thickness: 0.1 μm) in oxygen- and water-free atmosphere has been examined within the

potential window 1.2-3.7 V vs Li<sup>+</sup>/Li to check the electroactivity of the bare substrate. The first voltammogram of ITO (Figure 4) presents a broad reduction peak centered at about 1.75 V vs Li<sup>+</sup>/Li, which is accompanied by a second reduction process at about 1.2 V vs Li<sup>+</sup>/Li (sharp peak).

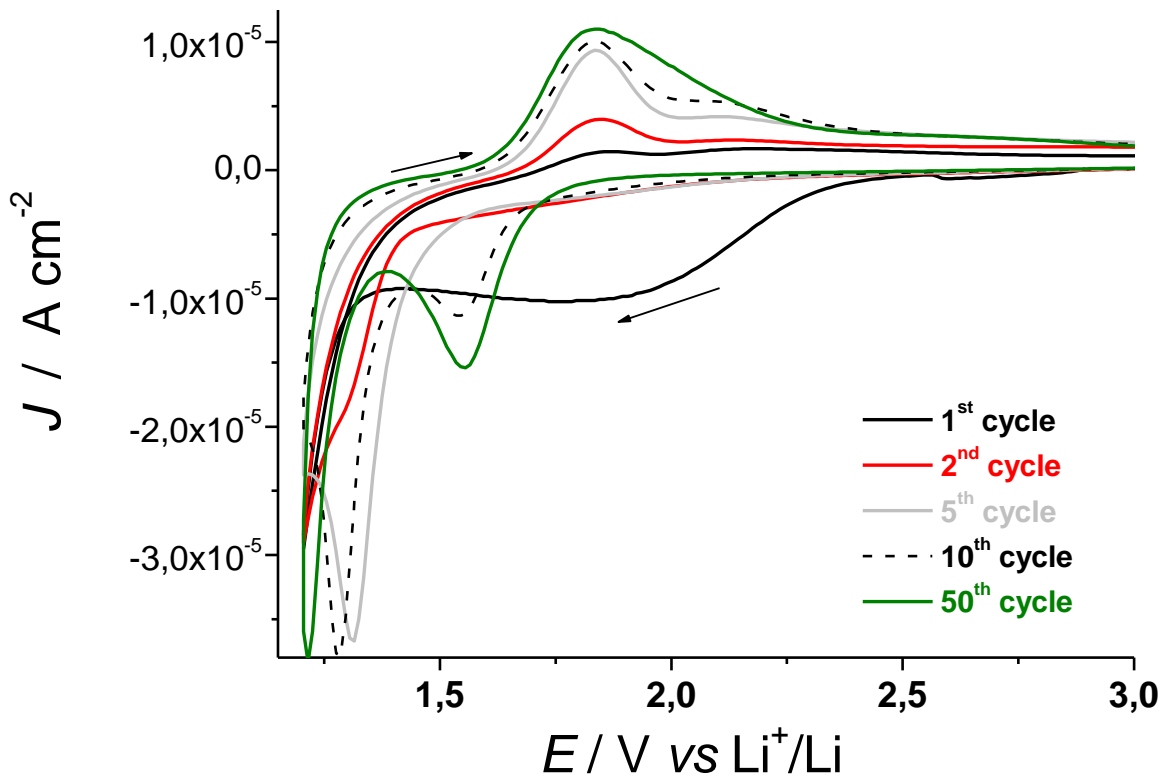
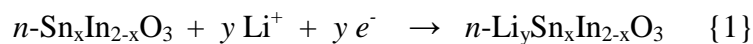


**Figure 4.** Evolution of the cyclic voltammogram of ITO. Electrolyte: 0.7 M LiClO<sub>4</sub> in anhydrous PC; counter electrode: Li; reference redox couple: Li<sup>+</sup>/Li; scan rate: 5 mV s<sup>-1</sup>.

On the basis of the sole analysis of the electrochemical results it is believed that the broad peak of reduction in the first cycle is associated with a process of lithium uptake (Eq.1) that brings about a severe rearrangement of ITO structure because of its irreversible character [26].



ITO lithiation (Eq.1) is equivalent to a *n*-doping process with occurrence of oxide reduction to a lower valence state of the metal centers. It is excluded the further reduction of the metal centers to a

fully reduced metallic state within the adopted range of applied potential. Beside chemical composition, the electroactivity of lithiated ITO (formula  $\text{Li}_y\text{-ITO}$ ) is also modified with respect to pristine ITO as evidenced by the differences between the first and second voltammogram (Figure 4). Upon further cycling the quasi-reversible reduction of bare ITO shifts to 1.31 V vs  $\text{Li}^+/\text{Li}$  and the exchange of a larger charge with respect to the second cycle is observed (Figure 4, scan 5). Further cycling (Figure 4, scans 10 and 50) leads to the observation of a new reduction peak at 1.54 V vs  $\text{Li}^+/\text{Li}$  the amplitude of which increases with the number of cycles. It is presumed that  $\text{Li}_y\text{-ITO}$  undergoes two distinct reduction processes consisting of lithium cations uptake at different surface sites of  $\text{Li}_y\text{-ITO}$ : the one at higher potential should refer to the uptake of lithium ions on  $\text{Li}_y\text{-ITO}$  surface directly exposed to the electrolyte whereas the one at lower potential is associated with the uptake of lithium ions in correspondence of the grain borders of  $\text{Li}_y\text{-ITO}$  in contact with the electrolyte.[10,37,38] The stable voltammogram of  $\text{Li}_y\text{-ITO}$  is obtained after several hundreds of cycles and is characterized by a broad reduction wave at around 1.5 V vs  $\text{Li}^+/\text{Li}$  comprising two poorly distinguishable redox processes (see Supplementary Information, Figure SI1). Since the ITO substrate participates in reduction processes and modifies irreversibly its transport properties when its potential is comprised in the range  $1.0 \leq E_{\text{appl}} \leq 2.6$  V vs  $\text{Li}^+/\text{Li}$  (Figure 4), only the process of electrochemical oxidation of  $\text{NiO}_x$  coatings on ITO can be examined without interferences from the substrate with  $\text{NiO}_x$  oxidation occurring within  $2.7 \leq E_{\text{appl}} \leq 3.7$  V vs  $\text{Li}^+/\text{Li}$  (Figure 5). Different to  $\text{NiO}_x$ , the ITO substrate possesses all metal centers in the highest oxidation state [In(III) and Sn(IV)] [36] and pronounced Faradaic currents associated with the further oxidation of In and Sn in ITO are not possible upon increase of the potential (Figure 4). The *n*-type nature of the ITO substrate might impose some limitations on the rate of those oxidation reactions occurring at potentials more positive than ITO flatband potential and generate a depletion region.[39] In fact, such a transport limitation is not verified since sintered  $\text{NiO}_x$  thin films on highly conductive degenerate ITO present their characteristic quasi-reversible oxidation peaked at approximately at 3.3 V vs  $\text{Li}^+/\text{Li}$  (Figure 5), the rate of which is limited by a  $\text{NiO}_x$  surface-confined process and not by a potential dependent electron-transfer process through  $\text{NiO}_x/\text{ITO}$  interface (*vide infra*).

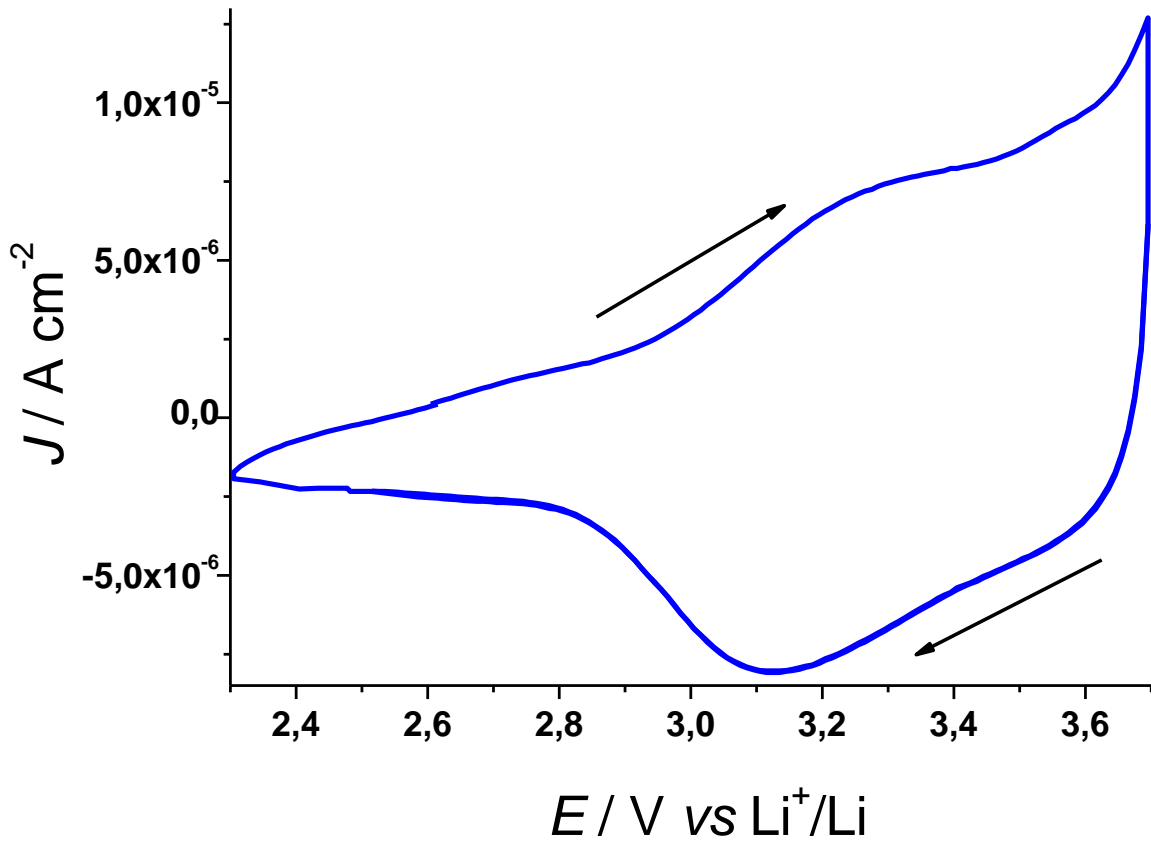
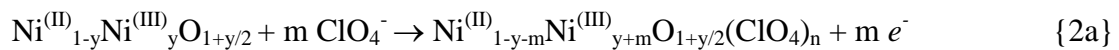
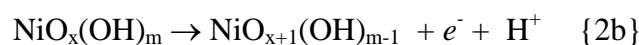


**Figure 5.** Cyclic voltammogram of NiO<sub>x</sub> coating deposited via sintering on ITO (thickness: 0.3 μm). Electrolyte: 0.7 M LiClO<sub>4</sub> in anhydrous PC; counter electrode: Li; reference electrode: Li<sup>+</sup>/Li; scan rate: 5 mV s<sup>-1</sup>.

Such an oxidation peak presents broad features and refers to the conversion of Ni(II) into Ni(III) in the oxide film [33]. Since the electrochemical reaction takes place in a solid phase, a more complete depiction of the whole redox process of NiO<sub>x</sub> in anhydrous electrolyte with LiClO<sub>4</sub> as depolarizer could be rewritten by the following equation where ClO<sub>4</sub><sup>-</sup> anion acts as charge-compensating species:



or alternatively



if nickel oxide is considered a mixture of oxide and hydroxide.[33] In both cases the electroactive  $\text{NiO}_x$  film is supposed to contain nickel ions in both oxidation states +2 and +3. In fact, the onset of NiO oxidation is about 2.85 V vs  $\text{Li}^+/\text{Li}$ . This indicates that the pristine film of sintered  $\text{NiO}_x$  already contains a fraction of Ni(III) sites since the open circuit voltage ( $V_{OC}$ ) of the cell

Glass/ITO/ $\text{NiO}_x$  // 0.7 M  $\text{LiClO}_4$  in PC // Li, Ref: Li/ $\text{LiClO}_4$  (0.7 M in PC) (a)

is 3.07 V vs  $\text{Li}^+/\text{Li}$ , i.e. a value which is above the onset of Ni(II) site oxidation. When the scan rate dependence of the more resolved reduction peak of sintered  $\text{NiO}_x$  is analyzed (Figure 6), a linear relationship between peak height and scan rate is found (see Supplementary Information, Figure SI4).

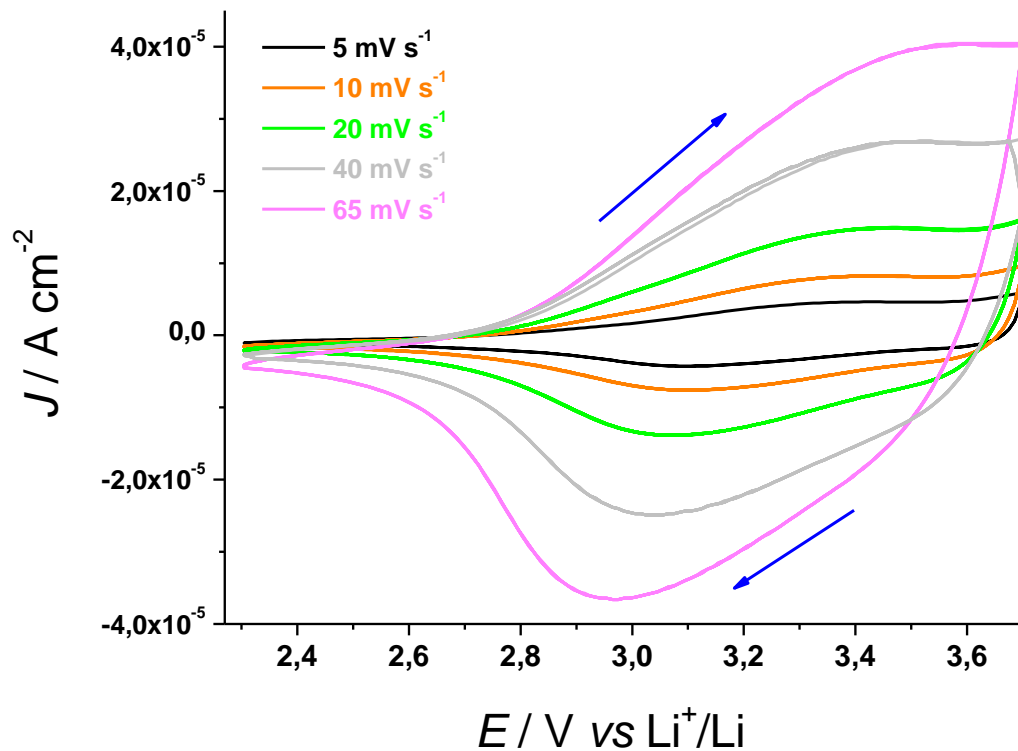


**Figure 6.** Cyclic voltammograms of the  $\text{NiO}_x$  coating (thickness: 0.3  $\mu\text{m}$ ) deposited via sintering of  $\text{NiO}_x$  nanoparticles on ITO at different scan rates. Cell configuration is the same as in Figure 5. Blue arrows indicate the direction of potential scan.

This corresponds to the occurrence of a surface confined redox process [40] the rate of which does not depend on the diffusion of charge carriers or mass transfer processes (*vide supra*), and is consistent with the previous data presented by Boschloo *et al.* who examined NiO<sub>x</sub> samples prepared via the sol-gel method.[33]

### 3.2 Photoelectrochemical characterization of ERY sensitized NiO<sub>x</sub>

The porous nature of the NiO<sub>x</sub> coatings deposited via sintering of oxide nanoparticles (Figure 1) renders possible the efficacious sensitization of the oxide with a visible light absorber. In the present work erythrosine B (ERY) has been considered as dye-sensitizer because of the matching of its frontier energy levels with the band edges of *p*-type NiO<sub>x</sub>. [13,24,27,41] Dye-sensitization of sintered NiO<sub>x</sub> sample with ERY generally leads to a small decrease of the dark current densities (Figure 7), with respect to the corresponding curves of bare nickel oxide samples (Figure 6). Moreover, current peaks associated with ERY-based electrochemical processes are not introduced in the voltammogram of ERY-sensitized NiO<sub>x</sub> deposited on ITO substrates within the experimental range of applied potential.

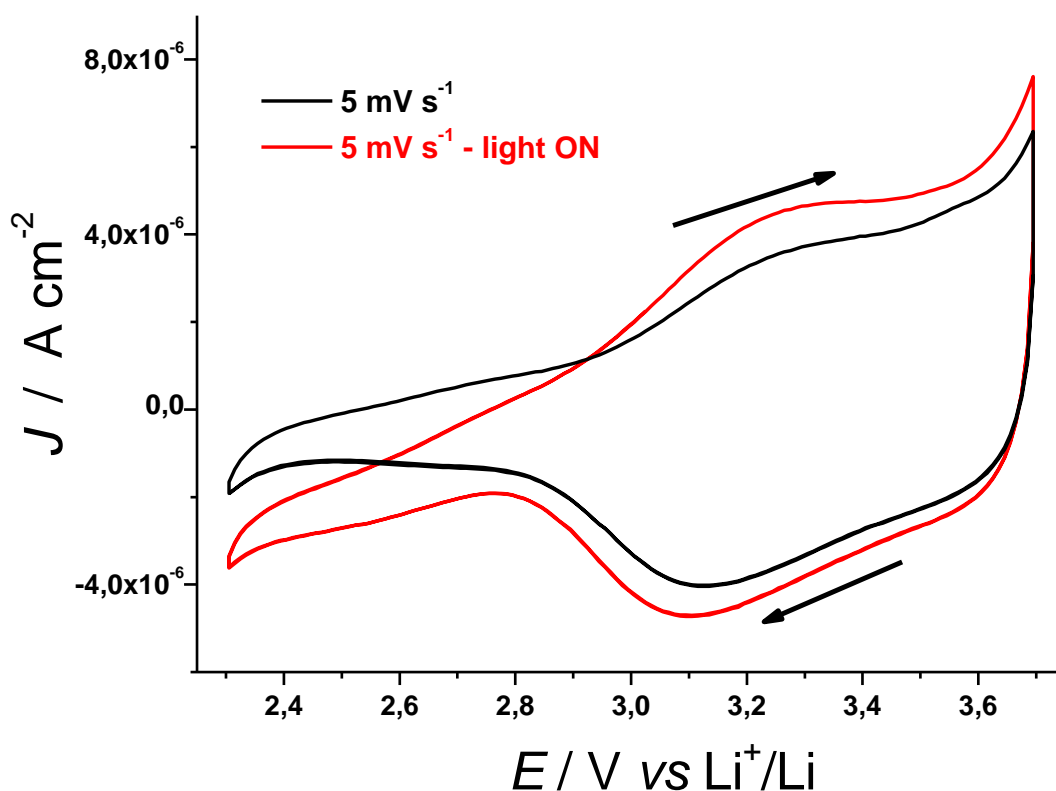


**Figure 7.** Cyclic voltammograms of the ERY-sensitized  $\text{NiO}_x$  coating (thickness:  $0.3 \mu\text{m}$ ) in the dark and under illumination with white light ( $P_{in} = 50 \text{ W}$ ) from an halogen lamp. Electrolyte composition as in Figure 5. Electrode area:  $1.75 \text{ cm}^2$ . Arrows indicate the direction of potential scan.

Therefore, ERY layer behaves as an electrochemically inert layer with no involvement in any of the observed faradic processes. Illumination of the dye-sensitized oxide samples with white light produces a positive photo-potential, an increase of the oxidation current density, and the negative shift of the current baseline when no redox processes occur (Figure 7). These facts can be explained in terms of photogeneration of positive charge carriers in dye-sensitized nickel oxide when visible light is absorbed by ERY layer (photoconductive effect).<sup>[13,24,41]</sup> Cyclic voltammetries of ERY-sensitized  $\text{NiO}_x$  have been carried out at different scan rates in the dark and under white light illumination (see Supplementary Information, Figures SI5 and SI6) in order to evaluate the characteristics of the dark and photo-oxidation process of  $\text{NiO}_x$  when sensitized.

The cathodic peak referring to the reverse process  $\text{Ni}^{(\text{III})} \rightarrow \text{Ni}^{(\text{II})}$  (reverse of processes in Eqs.2) has been considered for analysis because of its generally better resolution with respect to the correlated anodic peak which displays broader features in the voltammogram. Similar to bare  $\text{NiO}_x$ , both dark

and photo-electrochemical oxidation processes of ERY-sensitized  $\text{NiO}_x$  present the typical features of a surface confined redox process being the current peaks directly proportional to the scan rate (see Supplementary Information, Figure SI7).

ERY-sensitized  $\text{NiO}_x$  on ITO has been utilized as photoactive electrode in a cathodic DSC [24] with platinized indium-doped tin oxide (ITO) as counter electrode. The photocathode and the counter electrode had the same electroactive area in the DSC. The electrolyte was a solution of the redox couple  $\text{I}_3^- / \text{I}^-$  in acetonitrile. The characteristic curve of the  $\text{NiO}_x$  based cathodic DSC is presented in Figure 8.

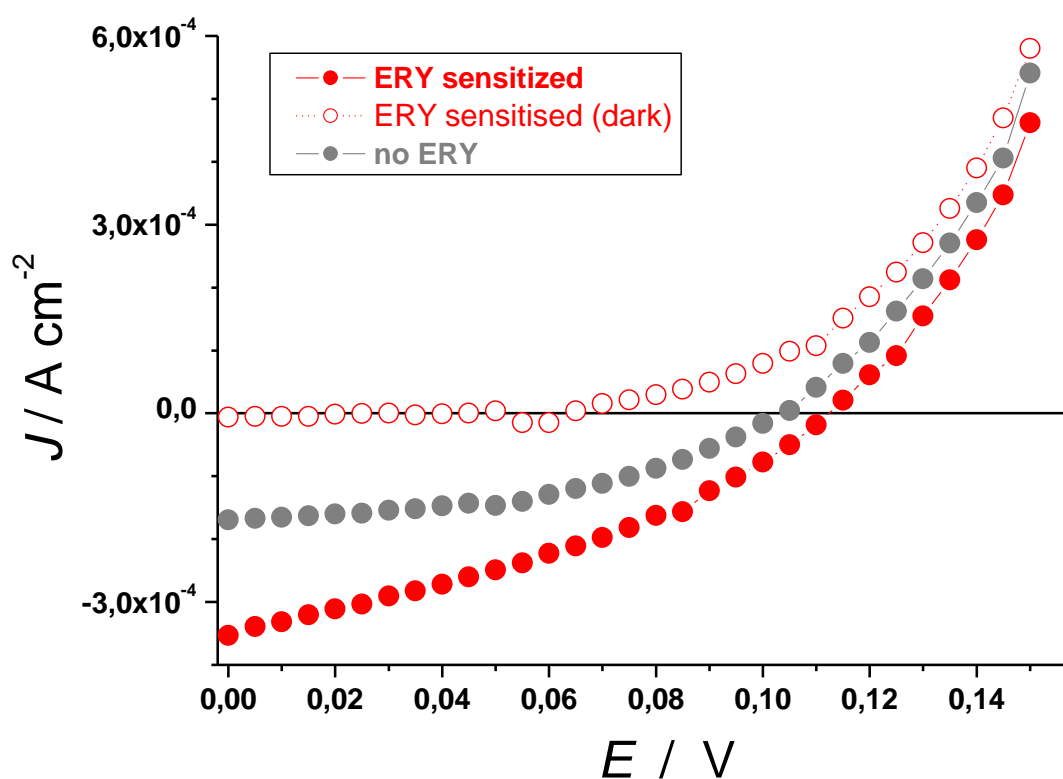


**Figure 8.** Characteristic  $J$ - $V$  curves of cathodic DSCs in  $\text{I}_3^-/\text{I}^-$  electrolyte for  $\text{NiO}_x$  in different states and conditions: i) bare state under illumination; ii) ERY-sensitized state under illumination; iii) ERY-sensitized state in the dark. Electroactive area:  $0.5\text{-}0.7\text{ cm}^2$ . The incident intensity of the sun simulator was  $0.1\text{ W cm}^{-2}$ . Prior sensitization the thickness of the  $\text{NiO}_x$  coating was  $0.6\text{ }\mu\text{m}$ .

The cathodic DSC based on photoactive sintered  $\text{NiO}_x$  showed an overall efficiency  $\eta = 0.014\%$  with open circuit voltage  $V_{OC} = 0.11\text{ V}$ , short circuit current density  $J_{SC} = -0.353\text{ mA cm}^{-2}$  and fill factor  $FF = 0.35$ . The influence of sensitization can be evaluated through the comparison of the characteristic curves recorded on illuminated  $\text{NiO}_x$  samples with and without sensitizer (Figure 8).

The resulting variations  $\Delta V_{OC}$  and  $\Delta J_{SC}$  in passing from the performance of bare  $NiO_x$  to that of ERY-sensitized  $NiO_x$  are respectively 9 mV and  $-1.83 \times 10^{-4} \text{ A cm}^{-2}$ . These results indicate that sensitization has a stronger influence on the kinetics-dependent term  $J_{SC}$  with respect to the thermodynamic parameter  $V_{OC}$ . It must be pointed out that the performance of bare  $NiO_x$  is comparable to that of the ERY sensitized cathode (Figure 8). This implies that the photo-generation of charge carriers in bare  $NiO_x$  following the absorption of the UV fraction of the impinging radiation [22] has non negligible effects. The sole effect of illumination is evaluable when the characteristic curves recorded on ERY-sensitized  $NiO_x$  in the dark and under illumination (Figure 8) are confronted. The parameter  $V_{OC}$  has an increment of 50 mV whereas the cathodic  $J_{SC}$  has an increase in module of  $3.47 \text{ A cm}^{-2}$  upon illumination of the cathodic DSC with  $0.1 \text{ W cm}^{-2}$  of sun simulator light. These results show a considerable improvement of the  $J$ - $V$  characteristic curve if compared to that of sol-gel prepared  $NiO_x$  films sensitized with the same dye,[13] which gave  $V_{OC} = 0.083 \text{ V}$ ,  $J_{SC} = -0.2 \text{ mA cm}^{-2}$ ,  $FF = 0.27$  and  $\eta = 0.0076 \%$  when  $1 \mu\text{m}$  thick  $NiO_x$  was tested. The improvements here reported are mainly ascribed to the better efficiency of sensitization in the  $NiO_x$  films obtained from the sintering of nanoparticles as a consequence of the enhanced mesoporosity (Figures 1 and 2) with respect to thin films of the same material prepared with wet methods.[14,21,23]

#### 4. Conclusions

This study has examined the electrochemical properties of  $NiO_x$  coatings ( $l < 3 \mu\text{m}$ ) on ITO, obtained using nanoparticle spray deposition/furnace sintering treatment.  $NiO_x$  coatings prepared via sintering of nanoparticles present a mesoporous morphology as a consequence of the nanoparticulate geometry retained after the thermal treatment. The oxidation of bare  $NiO_x$  coatings (solid state redox process) is not diffusion controlled but surface confined. It has been proved that the ITO substrate can get involved in cathodic redox processes that alter irreversibly the process of charge transfer through the ITO/ $NiO_x$  interface. For this reason the sole process of  $NiO_x$  electrochemical oxidation can be driven in absence of ITO substrate interference within the potential range  $2.7 \leq E_{appl} \leq 3.7 \text{ V vs Li}^+/\text{Li}$ . After sensitization with commercial erythrosine B the photo-electrochemical properties of the modified  $NiO_x$  coatings were analyzed for consideration of application in cathodic dye-sensitized solar cells. Again, in the sensitized state the oxidation of  $NiO_x$  is a surface confined process which is not modified by the presence of a monolayer of dye. The  $NiO_x$ -based DSCs displayed an improved  $J$ - $V$  performance with respect to  $NiO_x$  samples sensitized with the same dye but prepared with wet, not scalable methods displaying an overall

efficiency  $\eta = 0.014$  vs  $0.008$  % of sol-gel sample. The improvements obtained in this study are mainly ascribed to the better efficiency of sensitization as a consequence of the enhanced mesoporosity of NiO<sub>x</sub> films obtained using nanoparticle spray deposition followed by furnace sintering process.

## **Acknowledgements**

This material is based upon works supported by Science Foundation Ireland for the Solar Energy Conversion Strategic Research Cluster under Grant No. [07/SRC/B1160]. The authors acknowledge the assistance and support of industry partner Celtic Catalysts Ltd.

## **References**

1. Nalage SR, Chougule MA, Shashwati S, Joshi PB, Patil VB (2012) *Thin Solid Films* 520: 4835
2. Morrison SR, *Electrochemistry at semiconductor and oxidized metal electrodes*, Plenum Press, New York, 1980
3. Sato H, Minami T, Takata S, Yamada T (1993) *Thin Solid Films* 236: 27
4. Granqvist CG (2007) *Sol Energy Mater Sol Cells* 91: 1529
5. Nam KW, Yoon WS, Kim KB (2002) *Electrochim. Acta* 47: 3201
6. Lang JW, Kong LB, Liu M, Luo YC, Kang L (2010) *J Solid State Electrochem* 14: 1533
7. Estrada W, Andersson AM, Granqvist CG, Gorenstein A, Decker F (1991) *J Mater Res* 6: 1715
8. Svegl F, Surca-Vuk A, Hajzeri M, Slemenik-Perse L, Orel B *Sol (2012) Energy Mater Sol Cells* 99: 14
9. Avendaño A, Azens A, Niklasson GA, Granqvist CG (2007) *Mater Sci Engin B* 138: 112

10. Huang H, Tian J, Zhang WK, Gan YP, Tao XY, Xia XH, Tu JP (2011) *Electrochim Acta* 56: 4281
11. Gillaspie D, Norman A, Tracy CE, Pitts JR, Lee SH, Dillon A (2010) *J Electrochem Soc* 157: H328
12. Irwin MD, Buchholz DB, Hains AW, Chang RPH, Marks TJ (2008) *Proc Nat Acad Sci* 105: 2783
13. He J, Lindstrom H, Hagfeldt A, Lindquist SE (1999) *J Phys Chem B* 103: 8940
14. Nakasa A, Usami H, Sumikura S, Hasegawa S, Koyama T, Suzuki E (2005) *Chem Lett* 34: 500
15. Morandeira A, Boschloo G, Hagfeldt A, Hammarström L (2008) *J Phys Chem C* 112: 9530
16. Nattestad A, Ferguson M, Kerr R, Cheng YB, Bach U (2008) *Nanotechn* 19: 295304
17. Qin P, Zhu H, Edvinsson T, Boschloo G, Hagfeldt A, Sun L (2008) *J Am Chem Soc* 130: 8570
18. Li L, Gibson EA, Qin P, Boschloo G, Gorlov M, Hagfeldt A, Sun L, (2010) *Adv Mater* 22: 1759
19. Nattestad A, Mozer AJ, Fischer MKR, Cheng YB, Mishra A, Bauerle P, Bach U (2010) *Nature Mater* 9: 31
20. Awais M, Rahman M, MacElroy JMD, Coburn N, Dini D, Vos JG, Dowling DP (2010) *Surf Coat Techn* 204: 2729
21. Wu MS, Wang MJ (2010) *Chem Comm* 46: 6968
23. Garduño IA, Alonso JC, Bizarro M, Ortega R, Rodríguez-Fernández L, Ortiz A (2010) *J Cryst Growth* 312: 3276
23. Jiao Z, Wu M, Qin Z, Xu H (2003) *Nanotechn* 14: 458
24. He J, Lindstrom H, Hagfeldt A, Lindquist SE (2000) *Sol Energy Mater Sol Cells* 62: 265
25. (a) Cogan SF, Anderson EJ, Plante TD, Rauh RD (1985) *Appl Opt* 24: 2282; (b) Bressers PMMC, Meulenkaamp EA (1998) *J Electrochem Soc* 145: 2225
26. Wang Z, Hu X (2001) *Thin Solid Films* 392: 22

27. Awais M, Rahman M, MacElroy JMD, Dini D, Vos JG, Dowling DP (2011) *Surf Coat Techn* 205: S245
28. Halme J, Saarinen J, Lund P (2006) *Sol Energy Mater Sol Cells* 90: 887
29. Decker F, Passerini S, Pileggi R, Scrosati B (1992) *Electrochim Acta* 37: 1033
30. Masetti E, Dini D, Decker F (1995) *Sol Energy Mater Sol Cells* 39: 301
31. Gibson EA, Smeigh AL, Le Pleux L, Fortage J, Boschloo G, Blart E, Pellegrin Y, Odobel F, Hagfeldt A, Hammarström (2009) *Angew Chem Int Ed* 48: 4402
32. Mastroianni S, Lanuti A, Penna S, Reale A, Brown TM, Di Carlo A, Decker F (2012) *ChemPhysChem*, to be published
33. Boschloo G, Hagfeldt A (2001) *J Phys Chem B* 105: 3039
34. Passerini S, Scrosati B, Gorenstein A (1990) *J Electrochem Soc* 137: 3297
35. Passerini S, Scrosati B (1994) *J Electrochem Soc* 141: 889
36. Armstrong NA, Lin AWC, Masamichi F, Kuwana T (1976) *Anal Chem* 48: 741
37. Chippindale AM, Dickens PG, Powell AV (1991) *Prog Solid St Chem* 21: 133
38. Whittingham MS, Chen R, Chirayil T, Zavalij P (1997) *Solid State Ionics* 94: 227
39. Gerischer H (1990) *Electrochim Acta* 35: 1677
40. Bard AJ, Faulkner LR, *Electrochemical Methods (Fundamentals and Applications)*(2<sup>nd</sup> Ed.); John Wiley: New York, 2001; p.595
41. Vera F, Schrebler R, Munoz E, Suarez C, Cury P, Gomez H, Cordova R, Marotti RE, Dalchiele EA (2005) *Thin Solid Films* 490: 182